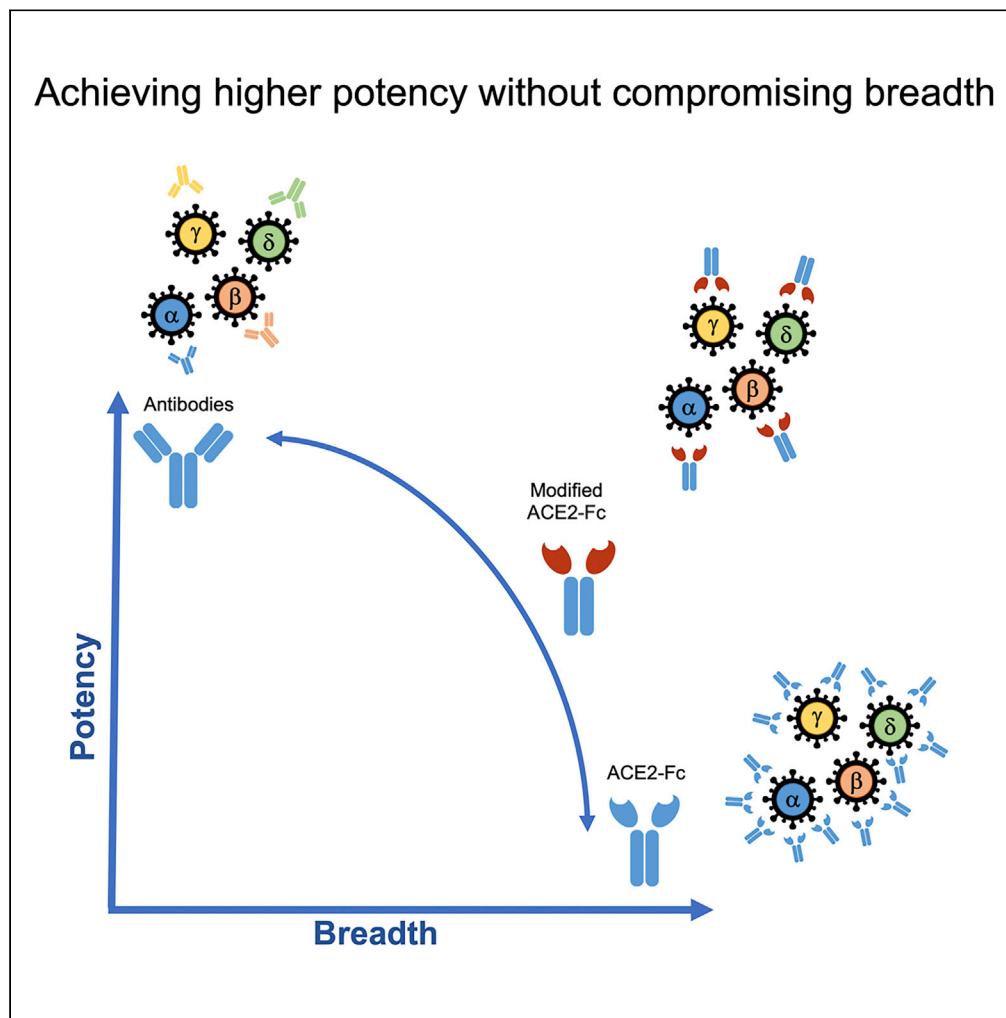## Article

Anti-SARS-CoV-2 immunoadhesin remains effective against Omicron and other emerging variants of concern

Hadas Cohen-Dvashi, Jonathan Weinstein, Michael Katz, ..., Nir Paran, Sarel Jacob Fleishman, Ron Diskin

ron.diskin@weizmann.ac.il

Highlights

ACE2-based immunoadhesins are a promising therapeutic tool against SARS-CoV-2

We employed a computational approach to design a superior ACE2 binder

An order of magnitude increase in neutralization capacity compared with human ACE2

The modified ACE2 retains efficacy against emerging variants of concern

iScience

Article

Anti-SARS-CoV-2 immunoadhesin remains effective against Omicron and other emerging variants of concern

Hadas Cohen-Dvashi,[1] Jonathan Weinstein,[2] Michael Katz,[1] Maayan Eilon-Ashkenazy,[1] Yuval Mor,[1] Amir Shimon,[1] Hagit Achdout,[3] Hadas Tamir,[3] Tomer Israely,[3] Romano Strobelt,[4] Maya Shemesh,[2] Liat Stoler-Barak,[5] Ziv Shulman,[5] Nir Paran,[3] Sarel Jacob Fleishman,[2] and Ron Diskin[1,6,*]

SUMMARY

Blocking the interaction of severe acute respiratory syndrome coronavirus 2 (SARS-CoV-2) with its angiotensin-converting enzyme 2 (ACE2) receptor was proved to be an effective therapeutic option. Various protein binders as well as monoclonal antibodies that effectively target the receptor-binding domain (RBD) of SARS-CoV-2 to prevent interaction with ACE2 were developed. The emergence of SARS-CoV-2 variants that accumulate alterations in the RBD can severely affect the efficacy of such immunotherapeutic agents, as is indeed the case with Omicron that resists many of the previously isolated monoclonal antibodies. Here, we evaluate an ACE2-based immunoadhesin that we have developed early in the pandemic against some of the recent variants of concern (VoCs), including the Delta and the Omicron variants. We show that our ACE2-immunoadhesin remains effective in neutralizing these variants, suggesting that immunoadhesin-based immunotherapy is less prone to escape by the virus and has a potential to remain effective against future VoCs.

INTRODUCTION

Coronavirus disease 2019 (COVID-19), caused by the severe acute respiratory syndrome coronavirus 2 (SARS-CoV-2), is an ongoing devastating pandemic leading to a substantial global death toll and an unprecedented economic loss. Since its emergence, SARS-CoV-2 accumulates changes that lead to the appearance of different variants (Harvey et al., 2021). Currently, the B.1.1.529 (Omicron) variant as well as its BA.4 and BA.5 sub-variants are rapidly spreading worldwide, causing significant morbidity and concern. Anti-SARS-CoV-2 vaccines (Baden et al., 2021; Polack et al., 2020; Voysey et al., 2021) revolutionized the way we combat the pandemic but many people, including both unvaccinated individuals and vaccinated people that lose protection over time, still contract the virus and may develop a serious, life-threatening disease. This problem seems to be especially pronounced with the Omicron-related variants. Therefore, there is still a pressing need to have a diversified set of good therapeutic options to alleviate the severity of the disease in hospitalized patients and reduce the likelihood of patients in high-risk groups from developing a serious illness.

Targeted immunotherapy against viral diseases emerged in recent years as a promising new therapeutic tool. Immunotherapy benefits from a dual action by both neutralizing viruses directly as well as recruiting immune effector functions for clearing infected cells. A monoclonal antibody (mAb) against the respiratory syncytial virus is effective and was approved for treating infected children (McLellan et al., 2010; Mejias and Ramilo, 2015). A breakthrough in the field of HIV was the isolation of broadly neutralizing mAbs (Scheid et al., 2011; Wu et al., 2010) and the affirmation of their use in treating (Caskey et al., 2017; Scheid et al., 2016) and protecting (Caskey et al., 2016; Wagh et al., 2016) individuals from HIV-1. In addition, antibodies against Lassa (Mire et al., 2017), Junin (Zeitlin et al., 2016), Ebola (Qiu et al., 2014), and even SARS (Greenough et al., 2005) viruses have been proven effective in animal models. Early in the COVID-19 pandemic, many mAbs were isolated (Cao et al., 2020; Ju et al., 2020; Kreer et al., 2020; Pinto et al., 2020; Robbiani et al., 2020; Rogers et al., 2020; Shi et al., 2020; Zost et al., 2020), and some were later formulated as immunotherapeutic reagents and/or cocktails like: bamlanivimab (Gottlieb et al., 2021), etesevimab (Gottlieb

[1]Department of Chemical and Structural Biology, Weizmann Institute of Science, Rehovot 7610001, Israel

[2]Department of Biomolecular Sciences, Weizmann Institute of Science, Rehovot 7610001, Israel

[3]Department of Infectious Diseases, Israel Institute for Biological Research, Ness-Ziona, Israel
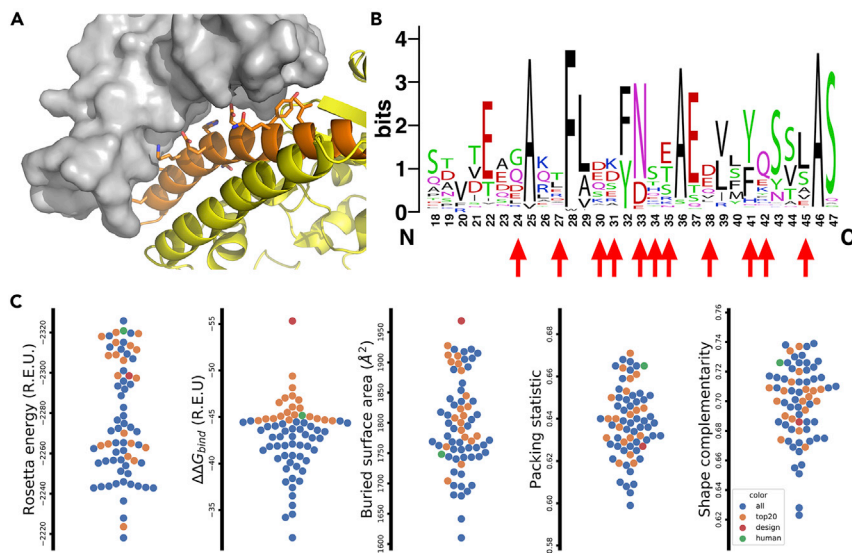
[4]Department of Molecular Genetics, Weizmann Institute of Science, Rehovot 7610001, Israel

[5]Department of Immunology, Weizmann Institute of Science, Rehovot 7610001, Israel

[6]Lead contact

*Correspondence:
ron.diskin@weizmann.ac.il
https://doi.org/10.1016/j.isci.2022.105193

Figure 1. Diversity of the SARS-CoV-2/ACE2 interface

(A) Structure of the SARS-CoV-2 RBD (gray surface) in complex with human-ACE2 (orange and yellow ribbon) (PDB: 6M17). The side chains of residues that make the recognition site for SARS-CoV-2 are shown as sticks. The N-terminal helix of ACE2 that makes the central part of the binding site is highlighted in orange.

(B) The sequence diversity of the first N-terminal helix of ACE2 in mammals is presented using a WebLogo display (Crooks et al., 2004). The abundance of the amino acid types in each position is represented by the height of their single-letter code. The residues that interact with the RBD of SARS-CoV-2 are indicated by red arrows.

(C) Interface properties of the various RBS/ACE2-ortholog models. Each dot represents a single model. From left to right, five panels show the calculated total Rosetta energy (using Rosetta energy units), the binding energy ($\Delta\Delta G$ for binding), the buried surface area, the packing statistics, and the shape complementarity of the interface. All the panels are arranged such that the values at the top represent better results. The RBD/human-ACE is indicated with a green dot. The modified ACE2 is indicated with a red dot.

et al., 2021), REGN-COV2 (Weinreich et al., 2021), sotrovimab (Gupta et al., 2021), and others. Alarmingly, a series of studies indicate a reduction in efficacy of these mAbs against the Omicron variant (Boschi et al., 2022; Cao et al., 2021; Chen et al., 2021a; Tada et al., 2021).

Immunoadhesins make another class of immunotherapeutic agents. These are antibody-like molecules that consist of an engineered binding domain fused to an Fc portion on an antibody (Capon et al., 1989). The viral cellular receptor could serve as a binding domain for constructing such immunoadhesins. Due to natural adaptation, however, zoonotic viruses may bind to their animal-derived ortholog cellular receptors at higher affinities than the human cell-surface receptors (Shimon et al., 2017). Thus, immunoadhesins that make use of host-ortholog receptors can provide superior antiviral therapeutics. We recently demonstrated this approach by constructing Arenacept, which is a powerful immunoadhesin that targets viruses from the *Arenaviridae* family of viruses (Cohen-Dvashi et al., 2020a). Early in the pandemic, we (Cohen-Dvashi et al., 2020b) and others (Case et al., 2020; Chan et al., 2020; Glasgow et al., 2020; Lei et al., 2020; Monteil et al., 2020; Mou et al., 2021; Tada et al., 2020) have used angiotensin-converting enzyme 2 (ACE2), which is the cellular receptor of SARS-CoV-2 (Li et al., 2003; Walls et al., 2020; Yan et al., 2020), to construct anti-SARS-CoV-2 immunoadhesins that neutralize the virus and mediate Fc-effector functions (Chen et al., 2021b). Here, we describe the construction of this engineered ACE2 immunoadhesin and show that it retains efficacy toward Omicron as well as other VoCs.

RESULTS

The binding of SARS-CoV-2 to its ACE2 receptors is mediated by the receptor-binding domain (RBD), which is part of its spike complex (Lan et al., 2020; Shang et al., 2020; Walls et al., 2020; Wrapp et al., 2020). ACE2 has a long helical segment at its N-terminus, which forms most of the RBD-recognition site on ACE2 (Figure 1A). A multiple sequence alignment of over 200 ACE2 sequences derived from mammals indicates that many of the ACE2 positions that comprise the SARS-CoV-2 recognition site
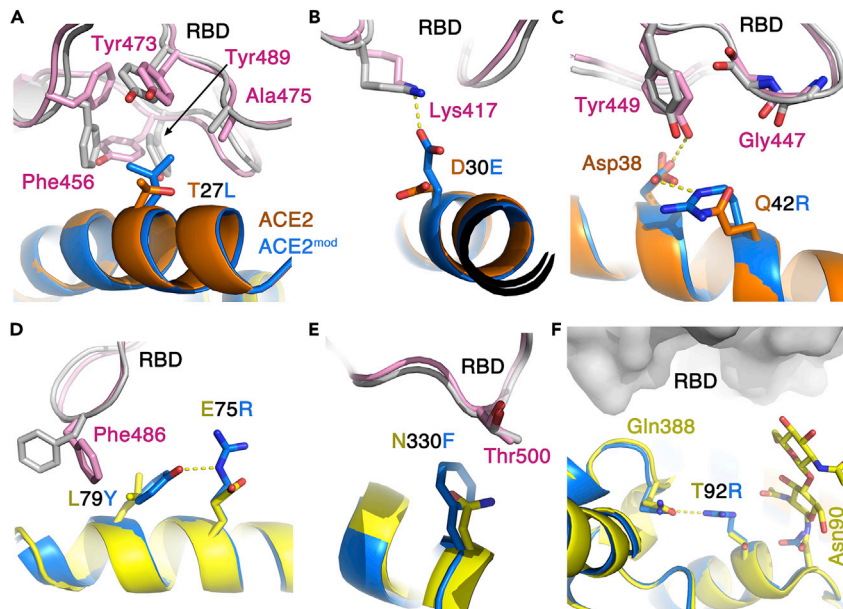
Figure 2. Optimized ACE2 interface for improved binding of SARS-CoV-2

The interfaces of SARS-CoV-2 RBD/human-ACE2 (gray and orange/yellow, respectively) and of the SARS-CoV-2 RBD/ modified-ACE2 (pink and light blue, respectively) are shown.

(A) Leucine, instead of threonine in position 27, makes better van der Waals interactions with hydrophobic residues on the SARS-CoV-2 RBD.

(B) Glutamic acid in position 30 of ACE2 can make a salt bridge with Lys417 of SARS-CoV-2, but not an aspartic acid that is present in the human-ACE2.

(C) Arginine in position 42 can form a salt bridge with Asp38 of ACE2 to stabilize it in a configuration that allows it to make a hydrogen bond with the hydroxyl of Tyr449 from SARS-CoV-2 RBD. An arginine in this position can also assume a different rotamer that will allow it to form electrostatic interaction with the main-chain carbonyl oxygen of Gly447 of SARS-CoV-2 RBD.

(D) A double replacement of Leu79 and Glu75 with tyrosine and arginine, respectively, allows favorable interaction between Phe486 of SARS-CoV-2 RBD and Tyr79 that is stabilized through a hydrogen bond by Arg75.

(E) Phenylalanine in position 330 of ACE2 is predicted to pack better against the aliphatic portion of Thr500 from SARS-CoV-2 RBD.

(F) A replacement of Thr92 with arginine abrogates the glycosylation site on Asn90, which bears a glycan that can sterically interfere with the binding of SARS-CoV-2 RBD. An arginine in position 92 of ACE2 can form a hydrogen bond with the nearby Gln388.

are not conserved (Figure 1B). This notion indicates an enormous putative sequence space that ACE2 can adopt.

To identify advantageous alterations of ACE2 that may enhance the binding to SARS-CoV-2, we selected 68 orthologous ACE2 genes with sequence identity to the human-ACE2 greater than 80% (Table S1). We used Rosetta atomistic modeling calculations (Methods S1) to assess the stability, binding energy ($\Delta\Delta G_{bind}$), interface packing, and shape complementarity for the RBD (starting from PDB entry 6VW1) (Figure 1C) (Shang et al., 2020). The computed binding energies correlate (Figure S1) with experimentally measured binding affinities (Wu et al., 2020). We visually inspected the top 20 models according to $\Delta\Delta G_{bind}$ and identified mutations that the calculations indicated would improve contacts with the SARS-CoV-2 RBD relative to the human-ACE2. Due to the high sequence diversity in ACE2, many design options were available. We rejected mutations to Trp, due to their tendency to form undesired promiscuous interactions and furthermore consulted a deep mutational sequencing dataset on ACE2 mutations and their impact on binding to the RBD (Procko, 2020). The vast majority of the suggested mutations were enriched in this mutational scanning, but a few potential mutations were not highly enriched and hence we eliminated them.

Three of the mutations that we decided to incorporate are located at the first N-terminal helix of human-ACE2. These three mutations include a T27L mutation that improves packing with hydrophobic residues of
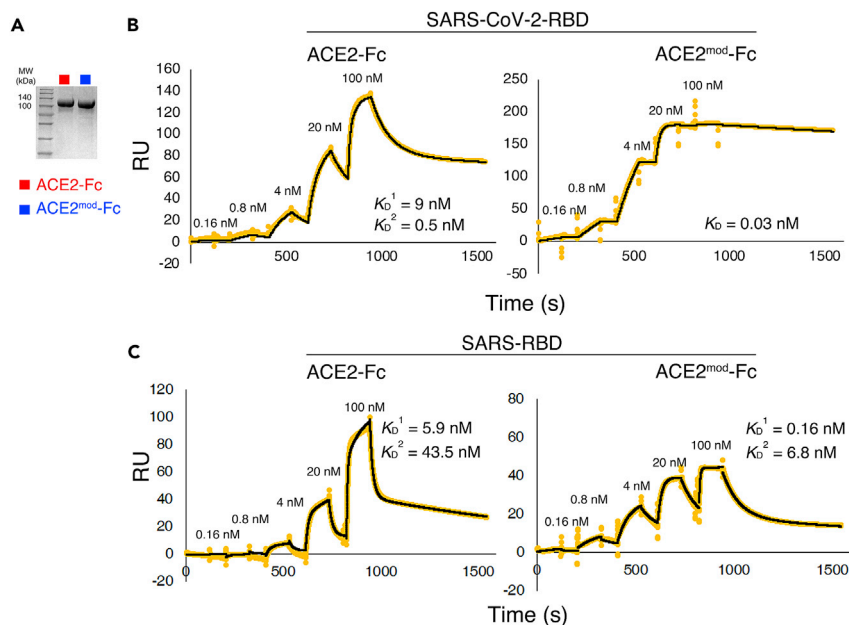
Figure 3. ACE2^{mod}-Fc is a superior binder of SARS-CoV-2

(A) Coomassie-stained SDS-PAGE showing ACE2-Fc and ACE2^{mod}-Fc.

(B and C) SPR analyses of SARS-CoV-2 RBD interaction with ACE2-Fc and ACE2^{mod}-Fc. Both ACE2-Fc and ACE2^{mod}-Fc were immobilized to a protein-A sensor chip and RBD from SARS-CoV-2 (B) and from SARS (C) were injected at the indicated concentration series using single-cycle kinetics experiments. Calculated dissociation constants are indicated. In the case of SARS-CoV-2 RBD binding to ACE2^{mod}-Fc, K_D was derived from a simple 1:1 binding model. In the case of SARS-CoV-2 RBD binding to ACE2-Fc, and the SARS RBD, the K_D values were derived using a heterogeneous-ligand binding model. These experiments were repeated twice and a representative sensorgram is shown for each.

SARS-CoV-2 RBD (Figure 2A), a D30E mutation that forms a new salt bridge with Lys417 of SARS-CoV-2 RBD (Figure 2B), and a Q42R mutation that may form a salt bridge with Asp38 of ACE2 and stabilize it in a configuration that favors the formation of a hydrogen bond with Tyr449 of SARS-CoV-2 RBD (Figure 2C). Alternatively, the new arginine may assume a different rotamer that makes favorable electrostatic interactions with the main-chain carboxylic oxygen of Gly447 from the SARS-CoV-2 RBD (Figure 2C). Besides these three mutations at the N-terminal helix of ACE2 that we selected, we identified two additional sites in the surrounding regions of ACE2. In the first site, we identified a putative change of Glu75 and Leu79 to arginine and tyrosine, respectively, that may interact favorably with Phe486 of SARS-CoV-2 RBD (Figure 2D). In the second site outside the first helix of ACE2, N330F may improve packing against the aliphatic portion of Thr500 from SARS-CoV-2 RBD (Figure 2E). We used Rosetta to model the combination of these six mutations and its impact on the binding to SARS-CoV-2 RBD. Our design showed a remarkable improvement in $\Delta\Delta G$ of binding as well as in the buried surface area (Figure 1C).

We decided to incorporate additional modification at other sites on top of modifying ACE2 residues that directly interact with SARS-CoV-2 RBD. Human-ACE2 has a putative glycosylation site at Asn90 that was shown to bear a glycan according to the SARS-CoV-2 RBD/human-ACE2 cryo-EM structure (Yan et al., 2020). This N-linked glycan projects toward the SARS-CoV-2 RBD, and presumably imposes steric constraints for the binding of SARS-CoV-2 RBD. The aforementioned deep mutational scanning dataset (Procko, 2020) is highly enriched with mutations in this N-linked glycosylation site, further supporting this notion. To eliminate this glycosylation site, we mutated Thr92 from the N-X-T glycosylation motif to an arginine that can make polar interactions with nearby glutamine (Figure 2F). Besides serving as a cellular receptor for SARS-CoV-2, ACE2 is an enzyme that has a critical biological function in regulating blood pressure by hydrolyzing angiotensin II (Keidar et al., 2007). While the enzymatic activity of ACE2 may protect from lung and cardiovascular damage (Imai et al., 2005; Kuba et al., 2006; Zoufaly et al., 2020), this activity may complicate the use of such ACE2-based reagent to fight viremia due to potential harmful effects of over conversion of angiotensin, when high doses are
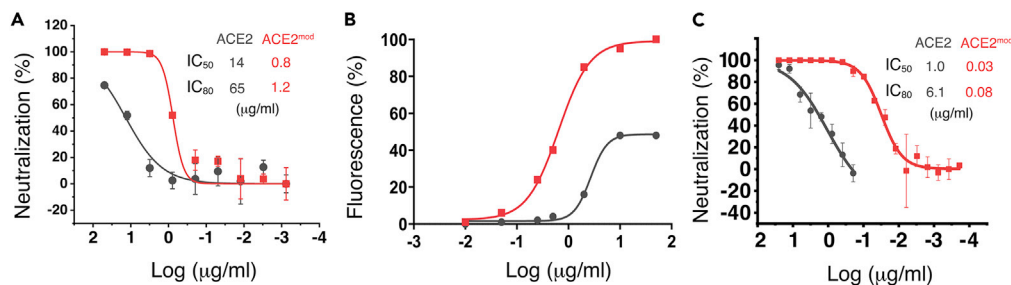
Figure 4. ACE2^{mod}-Fc exhibits improved biological activity in cells

(A) Neutralization of pseudotyped viruses by ACE2-Fc (gray) and ACE2^{mod}-Fc (red) is shown. The calculated IC$_{50}$ and IC$_{80}$ values are indicated. Error bars represent standard deviations. This experiment was repeated at least three times, and a representative graph is shown.

(B) Flagging of the SARS-CoV-2 spike complex on the cell surface. The concentration-depended ability of ACE2-Fc (gray) and ACE2^{mod}-Fc (red) to bind to surface-displayed SARS-CoV-2 spike complexes is analyzed using flow cytometry. Normalized overall fluorescence signals for the gate-selected cells are shown. This experiment was repeated three times, and a representative graph is shown.

(C) PRNT-determined neutralization of live SARS-CoV-2 by ACE2-Fc (gray) and ACE2^{mod}-Fc (red) is shown. The calculated IC$_{50}$ and IC$_{80}$ values are indicated. Error bars represent standard deviations of technical replicates. This experiment was performed once.

administrated. Hence, we decided to eliminate the catalytic activity of ACE2 by mutating its key catalytic position, Glu375, to leucine. Overall, we designed a variant that have a unique (Table S2) set of eight mutations.

To test our design, we produced two chimeric proteins that included amino acids 19–615 of the human-ACE2 ectodomain (omitting the original signal peptide) fused to an Fc portion of human IgG1, with or without the eight above-mentioned mutations (i.e., T27L, D30E, Q42R, E75R, L79Y, N330F, T92R, & E375L). Both the WT construct (ACE2-Fc) and our designed ACE2 construct (ACE2^{mod}-Fc) readily expressed as secreted proteins using HEK293F cells in suspension and were easily purified to near homogeneity using protein-A affinity chromatography (Figure 3A). Testing the enzymatic activity of both ACE2-Fc and ACE2^{mod}-Fc verified that the latter is indeed catalytic dead (Figure S2). We then immobilized the two immunoadhesins on a surface plasmon resonance sensor chip and used purified SARS-CoV-2 RBD as an analyte to determine their binding affinities. Noteworthy is this configuration that does not allow avidity. A simple 1:1 binding model gave a good fit for the binding data of ACE2^{mod}-Fc to SARS-CoV-2 RBD, but the binding of ACE2-Fc to SARS-CoV-2 RBD could not be fitted using this model, and we, therefore, used a more complex heterogeneous-ligand model that assumes some heterogeneity of the ACE2-Fc (Figure 3B). Such heterogeneity could presumably originate from partial glycosylation at Asn90 of ACE2. Remarkably, the binding affinity of ACE2^{mod}-Fc to SARS-CoV-2 RBD is more than two orders of magnitude stronger compared with the binding affinity of ACE2-Fc (Figure 3B). Moreover, although ACE2^{mod} was designed to bind SARS-CoV-2, we further tested its ability to bind the original SARS and found that not only it binds SARS-RBD but it aslo binds it with a significant higher affinity compared to ACE2-Fc (Figure 3C).

To test if the enhanced affinity of ACE2^{mod}-Fc could translate to improved biological functions, we conducted a pseudovirus neutralization assay using the spike complex of the original Wuhan-Hu-1 strain. The neutralization profile of ACE2^{mod}-Fc is apparently better compared to the profile of ACE2-Fc (Figure 4A). There is more than a 10-fold improvement in both IC$_{50}$ and IC$_{80}$ values, comparing the two reagents. Anti-SARS-CoV-2 immunoadhesin that binds to cell-surface displayed spike complexes might recruit beneficial immune factions via its Fc portion. We used flow cytometry to monitor the ability of ACE2-Fc and of ACE2^{mod}-Fc to stain HEK293 cells that transiently express the SARS-CoV-2 spike complex (Figure 4B). ACE2^{mod}-Fc has an apparent higher capacity to recognize the spike complex compared to ACE2-Fc. Achieving improved recognition of the SARS-CoV-2 spike complex prompted us to test the ability of ACE2^{mod}-Fc to directly neutralize live authentic viruses. For that, we performed plaque reduction neutralization test in a BSL-3 facility using the Wuhan-Hu-1 SARS-CoV-2 strain (Figure 4C). Both ACE2-Fc and ACE2^{mod}-Fc displayed better neutralization capacity of the live

Table 1. RBD mutations in recent VoC

Variant name	strain #	RBD mutations
Wuhan-Hu-1		-
Alpha	B1.1.7	N501Y
Beta	B1.351	K417N, E484K, N501Y
Gamma	P.1	K417T, E484K, N501Y
Delta	B1.672.2	L452R, T478K
Omicron	B1.592.1	K417N, N440K, G446S, S477N, T478K, E484A, Q493K, G496S, Q498R, N501Y, Y505H

viruses compared with the pseudoviral system (Figures 4A and 4C), and the potency of ACE2^{mod}-Fc was significantly higher compared to ACE2-Fc, achieving sterilizing effect well below 1 μg/mL. Hence, we managed to create a superior ACE2-based immunoadhesin that displays an improved capacity to target SARS-CoV-2.

Since its emergence as a human pathogen, SARS-CoV-2 is constantly changing by accumulating mutations. The changes that occur on the spike of the virus, and specifically on its RBD, have the potential to render anti-SARS-CoV-2 immunotherapeutic reagents, like ACE2^{mod}-Fc, ineffective. To explore this possibility, we generated pseudoviruses that contain the RBD mutations of the Alpha, Beta, Gamma, Delta, and Omicron VoCs (Table 1). Compared to the original Wuhan-hu-1 strain, ACE2^{mod}-Fc effectively neutralizes the Alpha, Beta, Gamma, and Delta VoCs (Figure 5A) that contain up to three alterations in their RBDs (Table 1). Unlike the other VoCs, the Omicron substantially differs from Wuhan-hu-1, having 11 relevant alterations in its RBD (Table 1). Nevertheless, ACE2^{mod}-Fc effectively neutralizes Omicron at the same efficiency as it neutralizes the Wuhan-hu-1 strain (Figure 5B). Thus, the VoCs that so far emerged do not reduce the neutralization capacity of ACE2^{mod}-Fc.

Avidity is a critical aspect that contributes to the potency of antibodies and antibody-like molecules (Cohen-Dvashi et al., 2020a; Klein and Bjorkman, 2010). Since the ACE2 receptor has a substantial size (Lan et al., 2020), we were concerned that the IgG1-derived hinge that links between the ACE2^{mod} and the Fc portion is not sufficiently long to enable both ACE2^{mod} arms to bind simultaneously. We therefore extended this hinge by three consecutive Gly-Ser-Gly-Gly repeats (ACE2$^{mod - GS3}$-Fc) and tested the effect of this extension on the capacity of neutralizing pseudotyped viruses. Extending the hinge significantly increased the neutralization potency (Figures 6A and 6B). The IC$_{50}$ values of ACE2$^{mod - GS3}$-Fc against both the Wuhan-Hu-1 and the Omicron strains are below 0.5 μg/mL (Figures 6A and 6B). Hence, the longer
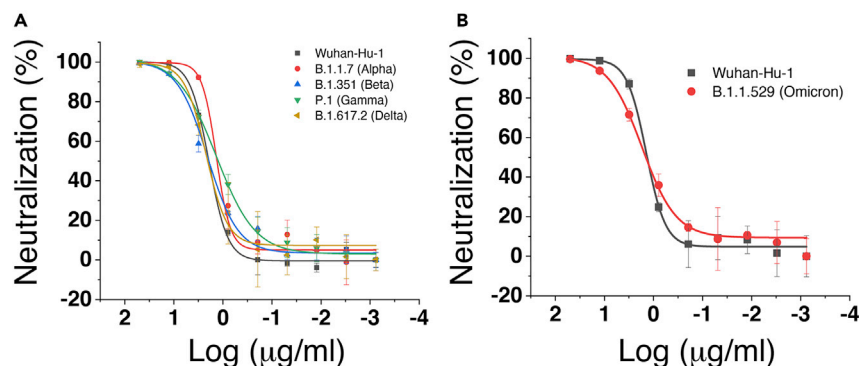
Figure 5. ACE2^{mod}-Fc retains activity against VoCs

(A) Neutralization of pseudotyped viruses with the spike complexes of the Alpha, Beta, Gamma, and Delta strains in comparison to Wuhan-Hu-1 strain by the ACE2^{mod}-Fc.

(B) Neutralization of pseudotyped viruses with the spike complexes of the Omicron vs. the Wuhan-Hu-1 strains by the ACE2^{mod}-Fc. These are representative neutralization curves of at least three independent repeats. Error bars represent standard deviations of technical replicates.
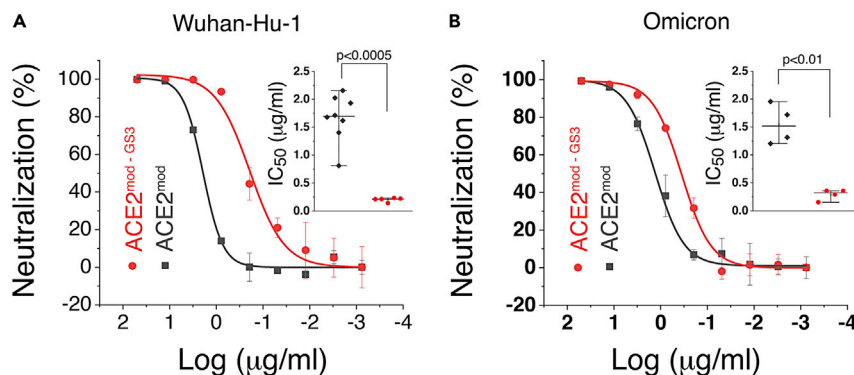
Figure 6. Extended hinge increases the potency of ACE2^{mod}-Fc

Neutralization of pseudotyped viruses with the spike complexes of Wuhan-Hu-1 (A) and of Omicron (B) by ACE2^{mod}-Fc (gray) and by ACE2$^{mod - GS3}$-Fc (red). Representative curves are shown. Error bars represent standard deviations of technical replicates. Insets show the difference in IC$_{50}$ values between ACE2^{mod}-Fc and ACE2$^{mod - GS3}$-Fc. Each dot is an IC$_{50}$ value calculated from an independent experiment. The p values (two-tailed Student's t test) are indicated.

hinge is better suited for allowing the two ACE2-arms of the immunoadhesin to bind simultaneously to achieve avidity.

DISCUSSION

Immunotherapy is an effective therapeutic tool for mitigating the disease severity and reducing the overall risk from SARS-CoV-2 infections in target populations. Although monoclonal antibodies reach exceptional potencies, they readily lose their efficacy due to changes that SARS-CoV-2 is accumulating. Ideally, we will want to progress into clinical development reagents that will stay effective for extended periods of time and against current circulating VoCs as well as ones that will emerge in the future. As we demonstrated here, it is possible to construct potent ACE2-based immunoadhesin that remains efficacious against emerging VoCs. Generally, while any modification of ACE2 opens a door for potential escape by the virus, the probability of such an event to happen will be lower compared to the probability of escape from monoclonal antibodies. This is due to the fact that ACE2^{mod}-Fc interacts solely with residues that are part of the ACE2-binding site whereas monoclonal antibodies inevitably make contacts with residues outside the binding site. While the virus can equally accumulate changes in all of its residues, changes in residues that make the ACE2-binding site, which may allow escape from ACE2^{mod}-Fc, have a significant higher probability to bear a fitness cost for the virus than residues outside the binding site. Therefore, the probability of the virus to escape monoclonal antibodies will be higher compared to ACE2-based immunoadhesins.

Along these lines, when this manuscript was submitted for publication, the Omicron BA.1 was the most prevalent VoC. While in revision, the BA.4 and BA.5 sub-variants became the dominant strains (Hachmann et al., 2022). These sub-variants have several changes in their RBD's compared to Omicron BA.1, including L452R, and F486V mutations and a reversion of R493 (a BA.1 mutation) back to a glutamine (Wuhan-Hu-1 sequence). These changes reduce the serum neutralization capacities of both vaccinated individuals and people who got infected with the Omicron BA.1 strain (Hachmann et al., 2022). While we do not have experimental data, structural analysis suggests that these changes will not affect the neutralization capacity of ACE2^{mod}-Fc. Specifically, L452R is a change occurring at a remote site that is not part of the ACE2-binding interface and thus is less likely to affect ACE2 binding. The reversion of Arg493 back to glutamine as in the sequence of Wuhan-Hu-1 makes it an ACE2^{mod}-Fc-compatible residue (Figure 4A). The F486V mutation replaces a large hydrophobic amino acid with a smaller hydrophobic amino acid (see Figure 2D) which might slightly reduce the overall affinity of the virus to ACE2, but could not interfere with the binding of ACE2^{mod}-Fc. Based on that, we predict that ACE2^{mod}-Fc will remain effective against the currently circulating VoCs.

Several ACE2-base immunoadhesins (Lei et al., 2020; Li et al., 2020; Tada et al., 2020), as well as phylogenetically-, library-, or structure-guided enhanced ACE2 (Chan et al., 2020; Glasgow et al., 2020; Mou et al., 2021) were previously described. Compared with these reported immunoadhesins, the ACE2$^{mod–GS3}$-Fc

that we present here is a highly potent reagent that has a different set of mutations (Table S2). Hence, the other reported immunoadhesins have orthogonal designs, which can allow us to diversify the immunotherapeutic toolkit against SARS-CoV-2. Such diversification could provide a safety net from losing immunotherapeutic options altogether in the possible scenario of the emergence of a resistance strain in the future.

Limitations of the study

The modified ACE2-based immunoadhesin that we present here was evaluated *in vitro*. Many promising reagents fail to ultimately demonstrate sufficient efficacy *in vivo* due to various, often unexpected, reasons. Additional experiments will be needed before a reagent like ACE2$^{mod-GS3}$-Fc could be considered for clinical use.

STAR★METHODS

Detailed methods are provided in the online version of this paper and include the following:

- KEY RESOURCES TABLE
- RESOURCE AVAILABILITY
  - Lead contact
  - Materials availability
  - Data and code availability
- EXPERIMENTAL MODEL AND SUBJECT DETAILS
  - Cell culture
- METHOD DETAILS
  - Atomistic modeling
  - Construction of expression vectors
  - Protein expression and purification
  - Surface plasmon resonance (SPR) measurements
  - Lentiviral particles production and neutralization
  - Flow cytometry analyses
  - ACE2 activity assay
  - Plaque reduction neutralization test (PRNT)
- QUANTIFICATION AND STATISTICAL ANALYSIS

AUTHOR CONTRIBUTIONS

R.D. conceived and oversaw the project; H.C.D. produced and analyzed ACE2-Fc and its variants; J.W. and S.J.F. performed computer-based modeling and analysis; R.S. established the pseudotyped viral neutralization assay; M.S. performed enzymatic activity assay; M.E-A. and Y.M. performed FACS analyses; M.K., M.E-A., and A.S. assisted in molecular biology and tissue culture efforts; H.A., H.T., T.I., and N.P. performed plaque reduction neutralization test.; L.S-B. and Z.S. performed supporting experiments; R.D. wrote the manuscript with the help of all other coauthors.

DECLARATION OF INTERESTS

The Weizmann Institute has filed for a patent for the ACE2^{mod}-Fc immunoadhesin.

REFERENCES

Altschul, S.F., Gish, W., Miller, W., Myers, E.W., and Lipman, D.J. (1990). Basic local alignment search tool. J. Mol. Biol. *215*, 403–410.

Amanat, F., Nguyen, T., Chromikova, V., Strohmeier, S., Stadlbauer, D., Javier, A., Jiang, K., Asthagiri-Arunkumar, G., Polanco, J., Bermudez-Gonzalez, M., et al. (2020). A serological assay to detect SARS-CoV-2 seroconversion in humans. Preprint at medRxiv. https://doi.org/10.1101/2020.03.17.20037713.

Baden, L.R., El Sahly, H.M., Essink, B., Kotloff, K., Frey, S., Novak, R., Diemert, D., Spector, S.A., Rouphael, N., Creech, C.B., et al. (2021). Efficacy and safety of the mRNA-1273 SARS-CoV-2 vaccine. N. Engl. J. Med. Overseas Ed. *384*, 403–416.

Boschi, C., Colson, P., Bancod, A., Moal, V., and Scola, B.L. (2022). Omicron variant escapes therapeutic mAbs contrary to eight prior main VOC. Preprint at bioRxiv. https://doi.org/10.1101/2022.01.03.474769.

Cao, Y., Su, B., Guo, X., Sun, W., Deng, Y., Bao, L., Zhu, Q., Zhang, X., Zheng, Y., Geng, C., et al. (2020). Potent neutralizing antibodies against SARS-CoV-2 identified by high-throughput single-cell sequencing of convalescent patients' B cells. Cell *182*, 73–84.e16.

Cao, Y., Wang, J., Jian, F., Xiao, T., Song, W., Yisimayi, A., Huang, W., Li, Q., Wang, P., An, R., et al. (2021). Omicron escapes the majority of existing SARS-CoV-2 neutralizing antibodies. Preprint at bioRxiv. https://doi.org/10.1101/2021.12.07.470392.

Capon, D.J., Chamow, S.M., Mordenti, J., Marsters, S.A., Gregory, T., Mitsuya, H., Byrn, R.A., Lucas, C., Wurm, F.M., Groopman, J.E., et al. (1989). Designing CD4 immunoadhesins for AIDS therapy. Nature *337*, 525–531.

Case, J.B., Rothlauf, P.W., Chen, R.E., Liu, Z., Zhao, H., Kim, A.S., Bloyet, L.M., Zeng, Q., Tahan, S., Droit, L., et al. (2020). Neutralizing antibody and soluble ACE2 inhibition of a replication-competent VSV-SARS-CoV-2 and a clinical isolate of SARS-CoV-2. Cell Host Microbe *28*, 475–485.e5.

Caskey, M., Klein, F., and Nussenzweig, M.C. (2016). Broadly neutralizing antibodies for HIV-1 prevention or immunotherapy. N. Engl. J. Med. *375*, 2019–2021.

Caskey, M., Schoofs, T., Gruell, H., Settler, A., Karagounis, T., Kreider, E.F., Murrell, B., Pfeifer, N., Nogueira, L., Oliveira, T.Y., et al. (2017). Antibody 10-1074 suppresses viremia in HIV-1-infected individuals. Nat. Med. *23*, 185–191.

Chan, K.K., Dorosky, D., Sharma, P., Abbasi, S.A., Dye, J.M., Kranz, D.M., Herbert, A.S., and Procko, E. (2020). Engineering human ACE2 to optimize binding to the spike protein of SARS coronavirus 2. Science *369*, 1261–1265.

Chen, J., Wang, R., Gilby, N.B., and Wei, G.W. (2021a). Omicron (B.1.1.529): infectivity, vaccine breakthrough, and antibody resistance. Preprint at arXiv. https://doi.org/10.48550/arXiv.2112.01318.

Chen, Y., Sun, L., Ullah, I., Beaudoin-Bussieres, G., Anand, S.P., Hederman, A.P., Tolbert, W.D., Sherburn, R., Nguyen, D.N., Marchitto, L., et al. (2021b). Engineered ACE2-Fc counters murine lethal SARS-CoV-2 infection through direct neutralization and Fc-effector activities. Preprint at bioRxiv. https://doi.org/10.1101/2021.11.24.469776.

Cohen-Dvashi, H., Amon, R., Agans, K.N., Cross, R.W., Borenstein-Katz, A., Mateo, M., Baize, S., Padler-Karavani, V., Geisbert, T.W., and Diskin, R. (2020a). Rational design of universal immunotherapy for TfR1-tropic arenaviruses. Nat. Commun. *11*, 67.

Cohen-Dvashi, H., Cohen, N., Israeli, H., and Diskin, R. (2015). Molecular mechanism for LAMP1 recognition by Lassa virus. J. Virol. *89*, 7584–7592.

Cohen-Dvashi, H., Weinstein, J., Katz, M., Eilon, M., Mor, Y., Shimon, A., Strobelt, R., Shemesh, M., Fleishman, S.J., and Diskin, R. (2020b). Coronacept – a potent immunoadhesin against SARS-CoV-2. Preprint at bioRxiv. https://doi.org/10.1101/2020.08.12.247940.

Crooks, G.E., Hon, G., Chandonia, J.M., and Brenner, S.E. (2004). WebLogo: a sequence logo generator. Genome Res. *14*, 1188–1190.

Das, R., and Baker, D. (2008). Macromolecular modeling with rosetta. Annu. Rev. Biochem. *77*, 363–382.

Edgar, R.C. (2004). MUSCLE: multiple sequence alignment with high accuracy and high throughput. Nucleic Acids Res. *32*, 1792–1797.

Glasgow, A., Glasgow, J., Limonta, D., Solomon, P., Lui, I., Zhang, Y., Nix, M.A., Rettko, N.J., Zha, S., Yamin, R., et al. (2020). Engineered ACE2 receptor traps potently neutralize SARS-CoV-2. Proc. Natl. Acad. Sci. USA *117*, 28046–28055.

Gordon, D.E., Jang, G.M., Bouhaddou, M., Xu, J., Obernier, K., White, K.M., O'Meara, M.J., Rezelj, V.V., Guo, J.Z., Swaney, D.L., et al. (2020). A SARS-CoV-2 protein interaction map reveals targets for drug repurposing. Nature *583*, 459–468.

Gottlieb, R.L., Nirula, A., Chen, P., Boscia, J., Heller, B., Morris, J., Huhn, G., Cardona, J., Mocherla, B., Stosor, V., et al. (2021). Effect of Bamlanivimab as monotherapy or in combination with Etesevimab on viral load in patients with mild to moderate COVID-19: a randomized clinical trial. JAMA *325*, 632–644.

Greenough, T.C., Babcock, G.J., Roberts, A., Hernandez, H.J., Thomas, W.D., Jr., Coccia, J.A., Graziano, R.F., Srinivasan, M., Lowy, I., Finberg, R.W., et al. (2005). Development and characterization of a severe acute respiratory syndrome-associated coronavirus-neutralizing human monoclonal antibody that provides effective immunoprophylaxis in mice. J. Infect. Dis. *191*, 507–514.

Gupta, A., Gonzalez-Rojas, Y., Juarez, E., Crespo Casal, M., Moya, J., Falci, D.R., Sarkis, E., Solis, J., Zheng, H., Scott, N., et al. (2021). Early treatment for covid-19 with SARS-CoV-2 neutralizing antibody Sotrovimab. N. Engl. J. Med. *385*, 1941–1950.

Hachmann, N.P., Miller, J., Collier, A.R.Y., Ventura, J.D., Yu, J., Rowe, M., Bondzie, E.A., Powers, O., Surve, N., Hall, K., and Barouch, D.H. (2022). Neutralization escape by SARS-CoV-2 Omicron subvariants BA.2.12.1, BA.4, and BA.5. N. Engl. J. Med. *387*, 86–88.

Harvey, W.T., Carabelli, A.M., Jackson, B., Gupta, R.K., Thomson, E.C., Harrison, E.M., Ludden, C., Reeve, R., Rambaut, A.; COVID-19 Genomics UK COG-UK Consortium, and Robertson, D.L. (2021). SARS-CoV-2 variants, spike mutations and immune escape. Nat. Rev. Microbiol. *19*, 409–424.

Imai, Y., Kuba, K., Rao, S., Huan, Y., Guo, F., Guan, B., Yang, P., Sarao, R., Wada, T., Leong-Poi, H., et al. (2005). Angiotensin-converting enzyme 2 protects from severe acute lung failure. Nature *436*, 112–116.

Ju, B., Zhang, Q., Ge, J., Wang, R., Sun, J., Ge, X., Yu, J., Shan, S., Zhou, B., Song, S., et al. (2020). Human neutralizing antibodies elicited by SARS-CoV-2 infection. Nature *584*, 115–119.

Keidar, S., Kaplan, M., and Gamliel-Lazarovich, A. (2007). ACE2 of the heart: from angiotensin I to angiotensin (1-7). Cardiovasc. Res. *73*, 463–469.

Klein, J.S., and Bjorkman, P.J. (2010). Few and far between: how HIV may be evading antibody avidity. PLoS Pathog. *6*, e1000908.

Kreer, C., Zehner, M., Weber, T., Ercanoglu, M.S., Gieselmann, L., Rohde, C., Halwe, S., Korenkov, M., Schommers, P., Vanshylla, K., et al. (2020). Longitudinal isolation of potent near-germline SARS-CoV-2-neutralizing antibodies from COVID-19 patients. Cell *182*, 1663–1673.

Kuba, K., Imai, Y., Rao, S., Jiang, C., and Penninger, J.M. (2006). Lessons from SARS: control of acute lung failure by the SARS receptor ACE2. J. Mol. Med. *84*, 814–820.

Lan, J., Ge, J., Yu, J., Shan, S., Zhou, H., Fan, S., Zhang, Q., Shi, X., Wang, Q., Zhang, L., and Wang, X. (2020). Structure of the SARS-CoV-2 spike receptor-binding domain bound to the ACE2 receptor. Nature *581*, 215–220.

Lei, C., Qian, K., Li, T., Zhang, S., Fu, W., Ding, M., and Hu, S. (2020). Neutralization of SARS-CoV-2 spike pseudotyped virus by recombinant ACE2-Ig. Nat. Commun. *11*, 2070.

Li, W., Moore, M.J., Vasilieva, N., Sui, J., Wong, S.K., Berne, M.A., Somasundaran, M., Sullivan, J.L., Luzuriaga, K., Greenough, T.C., et al. (2003). Angiotensin-converting enzyme 2 is a functional receptor for the SARS coronavirus. Nature *426*, 450–454.

Li, Y., Wang, H., Tang, X., Ma, D., Du, C., Wang, Y., Pan, H., Zou, Q., Zheng, J., Xu, L., et al. (2020). Potential host range of multiple SARS-like coronaviruses and an improved ACE2-Fc variant that is potent against both SARS-CoV-2 and SARS-CoV-1. Preprint at bioRxiv. https://doi.org/10.1101/2020.04.10.032342.

McLellan, J.S., Chen, M., Kim, A., Yang, Y., Graham, B.S., and Kwong, P.D. (2010). Structural basis of respiratory syncytial virus neutralization by motavizumab. Nat. Struct. Mol. Biol. *17*, 248–250.

Mejias, A., and Ramilo, O. (2015). New options in the treatment of respiratory syncytial virus disease. J. Infect. *71* (*Suppl 1*), S80–S87.

Mire, C.E., Cross, R.W., Geisbert, J.B., Borisevich, V., Agans, K.N., Deer, D.J., Heinrich, M.L., Rowland, M.M., Goba, A., Momoh, M., et al. (2017). Human-monoclonal-antibody therapy protects nonhuman primates against advanced Lassa fever. Nat. Med. *23*, 1146–1149.

Monteil, V., Kwon, H., Prado, P., Hagelkrüys, A., Wimmer, R.A., Stahl, M., Leopoldi, A., Garreta, E., Hurtado Del Pozo, C., Prosper, F., et al. (2020). Inhibition of SARS-CoV-2 infections in engineered human tissues using clinical-grade soluble human ACE2. Cell *181*, 905–913.e7.

Mou, H., Quinlan, B.D., Peng, H., Liu, G., Guo, Y., Peng, S., Zhang, L., Davis-Gardner, M.E., Gardner, M.R., Crynen, G., et al. (2021). Mutations derived from horseshoe bat ACE2 orthologs enhance ACE2-Fc neutralization of SARS-CoV-2. PLoS Pathog. *17*, e1009501.

Noy-Porat, T., Makdasi, E., Alcalay, R., Mechaly, A., Levy, Y., Bercovich-Kinori, A., Zauberman, A., Tamir, H., Yahalom-Ronen, Y., Israeli, M., et al. (2020). A panel of human neutralizing mAbs targeting SARS-CoV-2 spike at multiple epitopes. Nat. Commun. *11*, 4303.

Pinto, D., Park, Y.J., Beltramello, M., Walls, A.C., Tortorici, M.A., Bianchi, S., Jaconi, S., Culap, K., Zatta, F., De Marco, A., et al. (2020). Cross-neutralization of SARS-CoV-2 by a human monoclonal SARS-CoV antibody. Nature *583*, 290–295.

Polack, F.P., Thomas, S.J., Kitchin, N., Absalon, J., Gurtman, A., Lockhart, S., Perez, J.L., Pérez Marc, G., Moreira, E.D., Zerbini, C., et al. (2020). Safety and efficacy of the BNT162b2 mRNA covid-19 vaccine. N. Engl. J. Med. *383*, 2603–2615.

Procko, E. (2020). The sequence of human ACE2 is suboptimal for binding the S spike protein of SARS coronavirus 2. Preprint at bioRxiv. https://doi.org/10.1101/2020.04.07.024752.

Qiu, X., Wong, G., Audet, J., Bello, A., Fernando, L., Alimonti, J.B., Fausther-Bovendo, H., Wei, H., Aviles, J., Hiatt, E., et al. (2014). Reversion of advanced Ebola virus disease in nonhuman primates with ZMapp. Nature *514*, 47–53.

Robbiani, D.F., Gaebler, C., Muecksch, F., Lorenzi, J.C.C., Wang, Z., Cho, A., Agudelo, M., Barnes, C.O., Gazumyan, A., Finkin, S., et al. (2020). Convergent antibody responses to SARS-CoV-2 in convalescent individuals. Nature *584*, 437–442.

Rogers, T.F., Zhao, F., Huang, D., Beutler, N., Burns, A., He, W.T., Limbo, O., Smith, C., Song, G., Woehl, J., et al. (2020). Isolation of potent SARS-CoV-2 neutralizing antibodies and protection from disease in a small animal model. Science *369*, 956–963.

Scheid, J.F., Horwitz, J.A., Bar-On, Y., Kreider, E.F., Lu, C.L., Lorenzi, J.C.C., Feldmann, A., Braunschweig, M., Nogueira, L., Oliveira, T., et al. (2016). HIV-1 antibody 3BNC117 suppresses viral rebound in humans during treatment interruption. Nature *535*, 556–560.

Scheid, J.F., Mouquet, H., Ueberheide, B., Diskin, R., Klein, F., Oliveira, T.Y.K., Pietzsch, J., Fenyo, D., Abadir, A., Velinzon, K., et al. (2011). Sequence and structural convergence of broad and potent HIV antibodies that mimic CD4 binding. Science *333*, 1633–1637.

Shang, J., Ye, G., Shi, K., Wan, Y., Luo, C., Aihara, H., Geng, Q., Auerbach, A., and Li, F. (2020). Structural basis of receptor recognition by SARS-CoV-2. Nature *581*, 221–224.

Shi, R., Shan, C., Duan, X., Chen, Z., Liu, P., Song, J., Song, T., Bi, X., Han, C., Wu, L., et al. (2020). A human neutralizing antibody targets the receptor-binding site of SARS-CoV-2. Nature *584*, 120–124.

Shimon, A., Shani, O., and Diskin, R. (2017). Structural basis for receptor selectivity by the Whitewater Arroyo mammarenavirus. J. Mol. Biol. *429*, 2825–2839.

Tada, T., Fan, C., Chen, J.S., Kaur, R., Stapleford, K.A., Gristick, H., Dcosta, B.M., Wilen, C.B., Nimigean, C.M., and Landau, N.R. (2020). An ACE2 microbody containing a single immunoglobulin Fc domain is a potent inhibitor of SARS-CoV-2. Cell Rep. *33*, 108528.

Tada, T., Zhou, H., Dcosta, B.M., Samanovic, M.I., Chivukula, V., Herati, R.S., Hubbard, S.R., Mulligan, M.J., and Landau, N.R. (2021). Increased resistance of SARS-CoV-2 Omicron variant to neutralization by vaccine-elicited and therapeutic antibodies. Preprint at bioRxiv. https://doi.org/10.1101/2021.12.28.474369.

Voysey, M., Clemens, S.A.C., Madhi, S.A., Weckx, L.Y., Folegatti, P.M., Aley, P.K., Angus, B., Baillie, V.L., Barnabas, S.L., Bhorat, Q.E., et al. (2021). Safety and efficacy of the ChAdOx1 nCoV-19 vaccine (AZD1222) against SARS-CoV-2: an interim analysis of four randomised controlled trials in Brazil, South Africa, and the UK. Lancet *397*, 99–111.

Wagh, K., Bhattacharya, T., Williamson, C., Robles, A., Bayne, M., Garrity, J., Rist, M., Rademeyer, C., Yoon, H., Lapedes, A., et al. (2016). Optimal combinations of broadly neutralizing antibodies for prevention and treatment of HIV-1 clade C infection. PLoS Pathog. *12*, e1005520.

Walls, A.C., Park, Y.J., Tortorici, M.A., Wall, A., McGuire, A.T., and Veesler, D. (2020). Structure, function, and antigenicity of the SARS-CoV-2 spike glycoprotein. Cell *181*, 281–292.e6.

Weinreich, D.M., Sivapalasingam, S., Norton, T., Ali, S., Gao, H., Bhore, R., Musser, B.J., Soo, Y., Rofail, D., Im, J., et al. (2021). REGN-COV2, a neutralizing antibody cocktail, in outpatients with covid-19. N. Engl. J. Med. *384*, 238–251.

Wrapp, D., Wang, N., Corbett, K.S., Goldsmith, J.A., Hsieh, C.L., Abiona, O., Graham, B.S., and McLellan, J.S. (2020). Cryo-EM structure of the 2019-nCoV spike in the prefusion conformation. Science *367*, 1260–1263.

Wu, L., Chen, Q., Liu, K., Wang, J., Han, P., Zhang, Y., Hu, Y., Meng, Y., Pan, X., Qiao, C., et al. (2020). Broad host range of SARS-CoV-2 and the molecular basis for SARS-CoV-2 binding to cat ACE2. Cell Discov. *6*, 68.

Wu, X., Yang, Z.Y., Li, Y., Hogerkorp, C.M., Schief, W.R., Seaman, M.S., Zhou, T., Schmidt, S.D., Wu, L., Xu, L., et al. (2010). Rational design of envelope identifies broadly neutralizing human monoclonal antibodies to HIV-1. Science *329*, 856–861.

Yan, R., Zhang, Y., Li, Y., Xia, L., Guo, Y., and Zhou, Q. (2020). Structural basis for the recognition of SARS-CoV-2 by full-length human ACE2. Science *367*, 1444–1448.

Zeitlin, L., Geisbert, J.B., Deer, D.J., Fenton, K.A., Bohorov, O., Bohorova, N., Goodman, C., Kim, D., Hiatt, A., Pauly, M.H., et al. (2016). Monoclonal antibody therapy for Junin virus infection. Proc. Natl. Acad. Sci. USA *113*, 4458–4463.

Zost, S.J., Gilchuk, P., Case, J.B., Binshtein, E., Chen, R.E., Nkolola, J.P., Schäfer, A., Reidy, J.X., Trivette, A., Nargi, R.S., et al. (2020). Potently neutralizing and protective human antibodies against SARS-CoV-2. Nature *584*, 443–449.

Zoufaly, A., Poglitsch, M., Aberle, J.H., Hoepler, W., Seitz, T., Traugott, M., Grieb, A., Pawelka, E., Laferl, H., Wenisch, C., et al. (2020). Human recombinant soluble ACE2 in severe COVID-19. Lancet Respir. Med. *8*, 1154–1158.

STAR★METHODS

KEY RESOURCES TABLE

REAGENT or RESOURCE	SOURCE	IDENTIFIER
Antibodies		
Donkey anti-human IgG H&L (HRP)	ABCAM	ab102429
Alexa Fluor® 488 AffiniPure Donkey Anti-Human IgG, Fcγ fragment specific	Jackson ImmunoResearch	Cat# 709-545-098; RRID: AB_2340565
Bacterial and virus strains		
live authentic SARS-CoV-2	kindly provided by Bundeswehr Institute of Microbiology, Munich, Germany	GISAID: EPI_ISL_406862
Chemicals, peptides, and recombinant proteins		
ACE2 and ACE2mod RBD – Fc	This paper	N/A
SARS1 RBD	This paper	N/A
SARS-CoV2 RBD	This paper	N/A
Critical commercial assays		
Bright-Glo luciferase assay system	Promega	E2610
SensoLyte® 390 ACE2 Activity Assay Kit	ANASPEC	AS-72086
Experimental models: Cell lines		
HEK293T	ATCC	
FreeStyle™ 293-F Cells	ThermoFischer	R79007
Vero E6	ATCC	
hACE2-FLAG overexpressing HEK293T cells	Genscript	SC1394
Oligonucleotides		
For SARS1 RBD cloning: 5' - CGGGATCCCGGGTGGTACCCTCAGG 3'- GAAGTTGACGCATTGATTTTTTATG	This paper	N/A
For SARS-CoV2 RBD strains mutations: K417N 5' - CTGGACAAACAGGCAACATTGCTGACTACAAC K417T 5' - CTGGACAAACAGGCACGATTGCTGACTACAAC L452R 5'- GCAACTACAACTACCGCTACAGACTGTTCAG L452R 3' - CTGAACAGTCTGTAGCGGTAGTTGTAGTTGC E484K 5' -CCATGTAATGGAGTGAAGGGCTTCAACTG T478K 5' - CCAGGCTGGCAGCAAACCATGTAATGGAG T478K 3'- CTCCATTACATGGTTTGCTGCCAGCCTGG	This paper	N/A
g-Block for generation of Omicron SARS-CoV2 spike TGAGGTGAGACAGATTGCCCCTGGACAAACAG GCAACATTGCTGACTACAACTACAAACTGCCT GATGACTTCACAGGCTGTGTGATTGCCTGGA ACAGCAACAAGCTGGACAGCAAGGTGAGCG GCAACTACAACTACCTCTACAGACTGTTCAGG AAGAGCAACCTGAAACCATTTGAGAGGGACA TCAGCACAGAGATTTACCAGGCTGGCAACAA ACCATGTAATGGAGTGGCGGGCTTCAACTG TTACTTTCCACTCAAATCCTATAGCTTCCGACC AACCTATGGAGTGGGCCACCAACCATACAGG GTGGTGGTGCTGTCCTTTGAACTGCTCC	This paper (IDT)	N/A

Continued		
REAGENT or RESOURCE	SOURCE	IDENTIFIER
Recombinant DNA		
ACE2 or ACE2mod RBD – Fc in pHLSEC	This Paper (Genscript)	synthesis/A
SARS-CoV-2 (2019-nCoV) Spike ORF mammalian expression plasmid (Codon Optimized)	Sino Biological Inc.	VG40589-UT
His-tagged SARS-CoV-2 Receptor Binding Domain (RBD)	Krammer F. Lab	(Amanat et al., 2020)
Full-length human ACE2 pCDNA3.1	Hyeryun Choe Lab Addgene plasmid #1786	(Li et al., 2003)
pLVX-EF1alpha-SARS1-Spike-2xStrep-IRES-Puro	Weizmann *Forchheimer* plasmid Bank	(Gordon et al., 2020)
Software and algorithms		
Origin 8	OriginLab	
Muscle	Edgar (2004)	
Rosetta	Das and Baker (2008)	http://www.rosettacommons.org

RESOURCE AVAILABILITY

Lead contact

Further information and requests for resources and reagents should be directed to and will be fulfilled by the lead contact, Ron Diskin (ron.diskin@weizmann.ac.il).

Materials availability

All unique plasmids generated in this study are available from the lead contact with a completed Materials Transfer Agreement (MTA).

Data and code availability

The Rosetta script that was used in this study is included in the supplemental information.

A list of the ACE2 orthologous accession codes that were used for Rosetta modeling, are available as a Table S1.

Any additional information required to reanalyze the data reported in this paper is available from the lead contact upon request.

EXPERIMENTAL MODEL AND SUBJECT DETAILS

Cell culture

Adherent cell-lines: HEK293T and Vero E6 cells are from the global bioresource center ATCC. hACE2-FLAG overexpressing HEK293T cells were purchased from Genscript (Cat. No. SC1394). HEK293T cells were cultured in high glucose Dulbecco's modified Eagle medium (DMEM) supplemented with 10% fetal bovine serum (FBS; Gibco), MEM non-essential amino acids, 2 nM L-Glutamine, 100 U/mL penicillin sodium and 100 μg/mL streptomycin (Biological industries, Israel). Vero E6 cells were cultured in MEM supplemented with the upper mentioned supplements plus 12.5 Units/mL Nystatin (Biological Industries, Israel). hACE2-HEK293T were cultured in DMEM supplemented with 10% FCS and 1 μg/mL Puromycin (Sigma-Aldrich). All adherent cells were grown at 37°C under atmosphere of 5% CO_2. Suspension cell-line: FreeStyle 293-F Cells were purchased from ThermoFischer and were cultured in FreeStyle media (Gibco) under agitation at 37°C and an atmosphere of 8% CO_2.

METHOD DETAILS

Atomistic modeling

Orthologous sequences of ACE2 were collected by using a protein BLAST (Altschul et al., 1990) search of the human-ACE2 sequence at GenBank and filtering the results to mammalian origin, and to sequences with greater than 80% identity to human-ACE2. Sequences were aligned using MUSCLE (Edgar, 2004).

Using the Rosetta suit (Das and Baker, 2008), each sequence was threaded on the human-ACE2/Spike structure (PDB entry: 6VW1) and relaxed using sidechain packing and backbone, sidechain and rigid-body minimization subject to harmonic constraints on the Cα coordinates observed in the experimental structure. The ref2015 energy function was used in all calculations (xml and command line are provided in the supplemental information). 100 models were generated for each sequence and the best scoring one was used for comparisons and analyses.

Construction of expression vectors

Codon-optimized forms of human ACE2 binding region (amino acids 19–615) and modified ACE2 genes were chemically synthesized (Genscript), and were subcloned upstream of a human Fc region (derived from IgG1) as previously described (Cohen-Dvashi et al., 2015), or upstream of same Fc region, which was pre-cloned to contain three Gly-Ser-Gly-Gly (GSGG) at the N-terminus part of the hinge. Plasmid (pCMV3) encoding the Full-length Clone DNA of SARS-CoV-2 spike was purchased from Sino Biological, and subcloned to the same plasmid after removing 19AA from the C'-terminus (Δ19 S_covid-pCMV3, done by Lab of Yossi Shaul). Luciferase-pLenti6 and ΔR89 Ψ vectors for lentivirus production were a kind gift from the lab of Dr. Julia Adler (Prof. Shaul Lab, Weizmann Institute). The plasmid encoding the His-tagged SARS-CoV-2 Receptor Binding Domain (RBD) was a kind gift from Florian Krammer lab (Amanat et al., 2020). Full-length human ACE2 was a kind gift from Hyeryun Choe (Li et al., 2003) (Addgene plasmid #1786). His-tagged SARS-CoV1 RBD was generated by subcloning the DNA-coding RBD region (AA 306–527) from pLVX-EF1alpha-SARS1-Spike-2xStrep-IRES-Puro plasmid (a gift from Prof. Nevan Krogan, UCSF; obtained from the Weizmann *Forchheimer* plasmid Bank collection). Mutated strains of the SARS-CoV-2 spike were generated by PCR mutagenesis and amino acids substitution in the RBD region only. For the Alpha (B1.1.7) N501Y, For the Beta (B1.351) K417N, E484K, N501Y. For the Gamma (P.1) K417T, E484K, N501Y. For the Delta (B.1.671.2) L452R, T478K. For the Omicron (B.1.1.529), a G-Block gene fragment (IDT) containing RBD mutations K417N, N440K, G446S, S477N, T478K, E484A, Q493K, G496S, Q498R, N501Y, Y505H, was Gibson assembled (NEB) instead of the original RBD sequence.

Protein expression and purification

ACE-Fc fusion proteins and the His-tagged SARS-CoV-1 or 2 RBDs were expressed in suspension-HEK293F cells grown in FreeStyle media (Gibco). Transfections were done using 40 kDa polyethyleneimine (PEI-MAX; Polysciences) at 1 mg of plasmid DNA per 1 L of culture at a cell density of 10^6/mL. Media were collected six days post-transfection and supplemented with 0.02% (w/v) sodium azide and PMSF. SARS RBDs were buffer exchanged to Phosphate Buffered Saline (PBS) using a tangential flow filtration system (Millipore), and captured using a HiTrap IMAC FF Ni^{+2} (GE Healthcare) affinity column followed by size exclusion chromatography purification with a Superdex 200 10/300 increased column (GE Healthcare). Fc-Fusion proteins were isolated using HiTrap protein-A (GE Healthcare) affinity columns.

Surface plasmon resonance (SPR) measurements

Binding of SARS-CoV-2 RBD or SARS-CoV-1 RBD to ACE2 –Fc and ACE2^{mod}–Fc fusion proteins were measured using a Biacore T200 instrument (GE Healthcare). Fusion proteins were first immobilized at a coupling density of ~1000 response units (RU) on a series S sensor chip protein A (GE Healthcare) in PBS and 0.02% (w/v) sodium azide buffer. RBD was then injected at 0.16, 0.8, 4, 20, and 100 nM concentrations, at a flow rate of 60 μL/min. Single-cycle kinetics was performed for the binding assay. The sensor chip was regenerated using 10 mM glycine-HCl pH 1.5 buffer.

Lentiviral particles production and neutralization

Lentiviruses expressing S-Covid19 spikes or mutated spikes were produced by transfecting HEK293T cells with Luciferase-pLenti6, D19 S_covid-pCMV3 and DR89 Ψ vectors at 1:1:1 ratio, using Lipofectamine 2000 (Thermo Fisher). Media containing Lentiviruses was collected at 48h post-transfection, centrifuged at 600xg for 5 min for clarifying from cells, and aliquots were frozen at −80°C.

For neutralization assays, hACE2 overexpressing HEK293T cells (Genscript) were seeded on a poly-L-lysine pre-coated white, chimney 96-well plates (Greiner Bio-One). Cells were left to adhere for 4h, followed by the addition of S-covid19 lentivirions, which were pre-incubated with 4-fold descending concentration series of either ACE2–Fc or ACE2^{mod}–Fc. Luminescence from the activity of luciferase was measured 48 h post-infection using a TECAN infinite M200 pro plate reader after applying Bright-Glo reagent (Promega)

on cells. IC_{50} and IC_{80} values were derived by fitting four-parameters neutralization curve using Origin 8 (OriginLab).

Flow cytometry analyses

Flow cytometry was used to detect the binding between ACE2-Fc or $ACE2^{mod}$-Fc to the spike complex of SARS-CoV-2 on cells. HEK293T cells were seeded on 10-cm plates and transfected 24 h later with 5 μg of Δ19 S_covid-pCMV3 using Lipofectamine 2000 (Invitrogen). Cells' media were replaced 6 h later to full medium, i.e., DMEM (Biological Industries) supplemented with 1% Pen-Strep (v/v), 1% Glutamine (w/v), and 1% (v/v) MEM Non-essential amino acids. At 24 h post-transfection, cells were detached by pipetting and washed by centrifugation at 400xg for 5 min and re-suspension in PBS/0.5% BSA solution. To prevent unspecific binding, blocking was performed by incubation in PBS/1% BSA for 15 min. Cells were aliquoted and incubated with different concentrations of ACE2-Fc or $ACE2^{mod}$-Fc diluted in PBS/0.5% BSA: 50, 10, 2, 0.5, 0.25, 0.05, 0.01 μg/mL for 1 h, washed, and incubated with a 1:200 dilution of Alexa Fluor 488 donkey-*anti*-human secondary antibody for 30 min. Unstained cells and secondary antibody-stained cells were used as negative controls. Analyses were performed using an LSR II flow cytometer (BD Biosciences). Curve fitting were performed using GraphPad Prism.

ACE2 activity assay

ACE2 activity was evaluated using SensoLyte 390 ACE2 Activity Assay Kit (ANASPEC; cat# 72,086) according to the manufacturer's protocol. 10 ng or 100 ng of ACE2-Fc and $ACE2^{mod}$-Fc samples were compared blank control. Measurement of product formation (fluorogenic peptide cleavage) as a function of time was taken every 10 s.

Plaque reduction neutralization test (PRNT)

Testing neutralization of live authentic SARS-CoV-2 (SARS-CoV-2 (GISAID: EPI_ISL_406862), kindly provided by Bundeswehr Institute of Microbiology, Munich, Germany) was conducted using an essentially identical protocol as previously reported (Noy-Porat et al., 2020). Briefly, Vero E6 cells were seeded overnight at a density of 0.5×10^6 cells/well in 12-well plates. Immunoadhesin samples were 2-fold serially diluted in 400 μL of MEM supplemented with 2% (v/v) FBS, MEM non-essential amino acids, 2 nM L-Glutamine, 100 Units/mL Penicilin, 0.1 mg/mL streptomycin and 12.5 Units/mL Nystatin (Biological Industries, Israel). 400 μL containing 300 PFU/mL of SARS-CoV-2 were then added to the immunoadhesin solution and the mixture incubated at 37°C, 5% (v/v) CO_2 for 1 h. Monolayers were washed once with DMEM w/o FBS and 200 μL of each immunoadhesin-virus mixture was added in duplicates to the cells for 1 h. Virus mixture w/o immunoadhesin was used as control. 2 mL overlay [MEM containing 2% FBS and 0.4% (w/v) tragacanth (Sigma, Israel)] were added to each well and plates were further incubated at 37°C, 5% CO_2 for 48 h. The number of plaques in each well was determined following media aspiration, cells fixation and staining with 1 mL of crystal violet (Biological Industries, Israel). Percent neutralization was defined as 100 x [# of plaques in control – # of plaques in experiment]/([# of plaques in control). IC_{50} and IC_{80} values were determined by fitting a four-parameter neutralization curve using Origin 8 (OriginLab). Handling and working with SARS-CoV-2 was conducted in BSL3 facility in accordance with the biosafety guidelines of the IIBR.

QUANTIFICATION AND STATISTICAL ANALYSIS

Data analysis and IC_{50}/IC_{80} calculations of all neutralization assays were preformed using Origin pro. Values were derived from fitting a non-linear 4 parameters dose-response curve. Neutralization experiments were repeated at least three times. Error bars represent SE from 4 technical replicates within one representative experiment. p Values (in boxplot Figure 6) were obtained by comparing two IC_{50} groups (each IC_{50} value represents one experiment) using two-tailed Student's T-Test.